Available online at www.sciencedirect.com
SCIENCE DIRECT®
Journal of Magnetic Resonance 173 (2005) 254–258
JMR Journal of Magnetic Resonance
www.elsevier.com/locate/jmr

Velocity imaging by ex situ NMR

J. Perlo, F. Casanova, B. Blümich*

Institut für Technische und Makromolekulare Chemie, RWTH Aachen, D-52056, Germany

Received 11 November 2004; revised 11 November 2004
Available online 26 January 2005

Abstract

A pulsed field gradient stimulated spin-echo NMR sequence is combined with imaging methods to spatially resolve velocity distributions and to measure 2D velocity maps ex situ. The implementation of these techniques in open sensors provides a powerful non-invasive tool to measure molecular displacement in a large number of applications inaccessible to conventional closed magnets. The method is implemented on an open tomograph that provides 3D spatial localization by combining slice selection in the presence of a uniform static magnetic field gradient along the depth direction with pulsed field gradients along the two lateral directions. Different pipe geometries are used to demonstrate that the sequence performs well even in the extremely inhomogeneous B_0 and B_1 fields of these sensors.

Keywords: Single-sided NMR; Mobile probes; Flow imaging; Ex situ NMR

1. Introduction

The combination of pulsed-field-gradient nuclear magnetic resonance (PFG NMR) methods with imaging techniques is a unique experimental tool to spatially resolve velocity distributions in optically non-transparent media [1–5]. It is applied in a rage of fields such as materials science, biology, chemical engineering, and petroleum engineering, where it is implemented to characterize the dynamics of complex fluids non-invasively [6–8]. These experiments are mainly carried out in the laboratory, since they require the high and homogeneous fields generated by superconducting magnets. However, this requirement severely limits the widespread use of the technique. Furthermore, conventional NMR magnets offer limited space to fit the sample or flow setup, and cannot easily be applied to study on-line different processing steps like transport, mixing, and extrusion. During the last years the interest in ex situ experiments has grown and new sensors based on open magnet geometries especially adapted to fit the object under study have been developed [9–13]. They offer excellent versatility in accessing a large number of applications inaccessible to closed magnet geometries. However, the price paid to gain this access is the generation of rather inhomogeneous magnetic fields across the sample under study, a fact that reduces the performance of conventional pulse sequences and request the design of special methods suitable to operate under these conditions [13–15].

Several problems appear, for example, when implementing a PFG sequence in extremely inhomogeneous magnetic fields like the ones provided by these sensors. First, the presence of static gradients of the order of some T/m gives rise to significant signal attenuation due to molecular self-diffusion. Second, the combination of large resonance offsets with inhomogeneous B_1 fields makes it impossible to define uniform plane rotations by RF pulses, introducing severe distortions in velocity measurements. Third, the low field (~10 MHz) and the broadband signal characteristic of open sensors lead to low sensitivity that extends the experimental times to unviable limits.

* Corresponding author. Fax: +49 241 8022185.
E-mail address: bluemich@mc.rwth-aachen.de (B. Blümich).

1090-7807/$ - see front matter © 2004 Elsevier Inc. All rights reserved.
doi:10.1016/j.jmr.2004.12.010

Recently, we have demonstrated that by implementing a modified PFG-STE sequence in an optimized single-sided sensor, these problems can be overcome to remotely measure velocity distributions in short experimental times. In this work this PFG-STE sequence is combined with imaging techniques to spatially resolve velocity distributions and to obtain 2D velocity maps ex situ. To illustrate the performance of the technique, the velocity distributions of liquids undergoing laminar flow in different pipe geometries are imaged using an open tomograph.

2. The velocity imaging method

Although the original PFG-STE sequence of Tanner [16] has been widely implemented to characterize flow in homogeneous fields, it strongly suffers from diffusion attenuation in the presence of background gradients. A more sophisticated version, the 13-interval sequence (*encoding period* in Fig. 1), divides the coding intervals by including π pulses that refocus the magnetization spread due to the static gradient G_0 [17]. In contrast to the PFG-STE, the diffusive signal attenuation due to G_0 takes place only during the coding periods δ but not during the evolution time Δ. Although the 13-interval sequence has been shown to perform well, we have recently demonstrated that its implementation on a single-sided sensor is not straightforward [15]. In the presence of highly inhomogeneous B_0 and B_1 fields, RF pulses do not define uniform plane rotations giving rise to a number of coherence pathways where the displacement is badly encoded. In our previous work, a proper phase cycle to efficiently remove the distortions coming from the unwanted pathways was presented. Furthermore, to improve the poor signal-to-noise ratio inherent to these sensors a novel multi-echo acquisition scheme was implemented [13]. By adding the echoes generated during the acquisition train, the experimental time could be significantly reduced. In this way velocity distributions could be measured at distances of up to 1 cm from the sensor surface in experimental times of a few minutes.

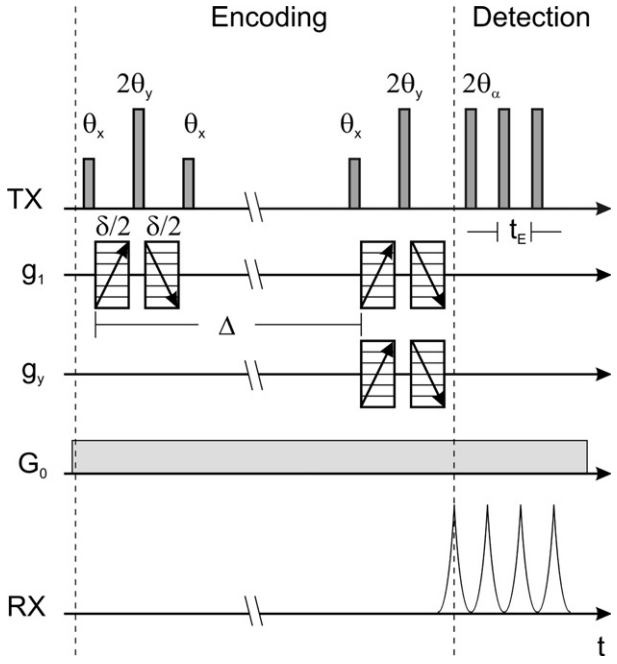

Fig. 1. 13-Interval stimulated spin-echo PFG sequence to measure displacement during the free evolution period Δ. To cancel the phase spread due to the static gradient generated by the open magnet geometry, refocusing 2θ pulses are applied during the coding intervals. The bipolar gradient pulses define an effective phase proportional to δg_1, where g_1 is the velocity encoding gradient amplitude. To increase the sensitivity a train of RF pulses (detection period) is applied after the formation of the stimulated echo. The echo time t_E for detection is determined by the dead time of the probe. The sequence includes a bipolar gradient pulse applied before the detection train to obtain spatial resolution along y.

In this work, the method developed to encode velocity is combined, first with slice selective imaging to spatially resolve the velocity profile in the object along the depth direction z (Fig. 2). The sensor used to implement this technique is equipped with a magnet optimized to generate a uniform static gradient along z. In the presence of such a gradient flat slices can be selected at different depth by stepping the excitation frequency. In general this step in frequency is chosen to move the slice position a distance equal to the slice thickness. As a second part of this work, a pulsed field gradient g_y is included in the sequence (Fig. 1) to resolve along y the velocity distribution inside a selected slice. Stepping the amplitudes of g_1 and g_y independently in a two-dimensional experiment the velocity distribution in each pixel along y can be determined. By combining this method with the slice selection procedure the velocity distribution in each pixel of the 2D image can be obtained. But this results in a time consuming three-dimensional experiment.

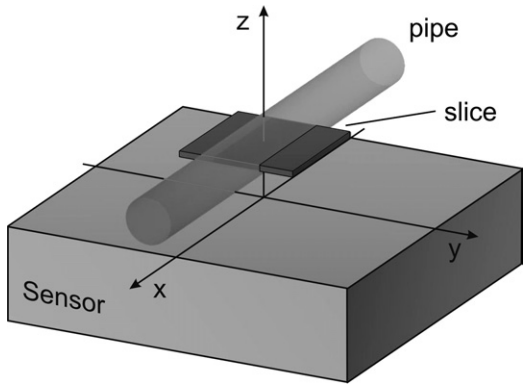

Fig. 2. Schematic of the sensor exciting a flat slice within the sample. The velocity profile in the sample can be spatially resolved along z by combining the sequence of Fig. 1 with retuning of the excitation frequency. Furthermore, a 2D velocity map can be reconstructed by including a pulsed gradient along y in the sequence.

In general the velocity distribution along x can be considered constant, so that a single velocity can be expected in each pixel of the image. In these cases a single phase-encoding step can be used for g_1 instead of the N steps needed to reconstruct the full propagator [15,18]. The procedure requires two imaging experiments with different g_1 amplitudes, thus in each pixel of the 2D image a phase shift proportional to the displacement is introduced. From the phase shift the velocity in each pixel can be easily computed to reconstruct a 2D velocity map of the cross section perpendicular to the flow direction.

As for the propagator measurements, the multi-echo acquisition scheme (*detection period* in Fig. 1) can also be implemented to reduce the experimental time in the sequences described above. In general, the train of refocusing pulses preserves the component of the echo signal parallel to the RF field, while the perpendicular component goes to zero after a transient period. To sample both components two experiments are performed, switching the phase α of the refocusing pulses from x to y. The full complex signal is then obtained by combining the x component of the first experiment with the y component of the second one [13]. As described in our previous work [15], a minimum of eight scans is required for the phase cycle to remove the distortions introduced by the flip-angle distribution defined by the rf pulses, and to sample the two components of the signal. For all experiments presented in this work the sensitivity enhancement achieved with the multi-echo acquisition scheme allowed us to use the minimum number of scans.

3. Experiments and results

The experiments presented in this section were conducted in an open tomograph that provides 3D spatial localization by combining slice selection in the presence of a uniform static gradient along the depth direction, with pulsed field gradients along the two lateral directions x and y. The proton resonance frequency at the surface of the sensor is about 8 MHz and the penetration depth goes up to 10 mm. In this region the static gradient is constant with a value of 2.5 T/m [13].

3.1. Spatially resolved velocity distributions

To illustrate the performance of the method to spatially resolve velocity distributions along z, the profile of water flowing in a rectangular pipe 30 mm wide, and 3 mm high was measured. A volume flow rate of 3600 ml/h was driven by a precision pump to define a maximum velocity in the pipe of about 17 mm/s. When the ratio b/a between the height and the width of the tube is much larger than 1, the velocity of laminar flow can be considered to be constant along the long side b while it changes as a quadratic function of the height a. The pipe was scanned along z by sweeping the position of the sensitive slice in steps of 0.3 mm from 7 to 10 mm, where the tube was placed. Fig. 3A shows the spatially resolved velocity distribution where the parabolic profile is clearly visible. Fig. 3B shows the propagators measured at three different positions in the tube. They show how the averaged velocity in the slice goes to zero as the slice approach the wall, while the width of the distributions increases, in agreement with the change in the velocity shear.

As a second example the velocity distribution of water flowing in a circular pipe with 3 mm inner diameter was scanned with the same experimental parameters as before. Fig. 4A shows the propagator spatially resolved along z. In contrast to the rectangular geometry, for a circular pipe of radius R the velocity depends on

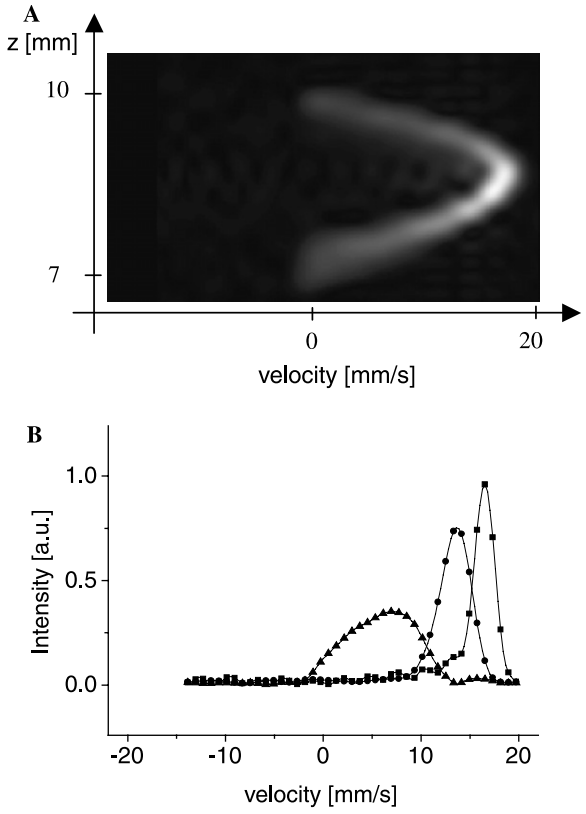

Fig. 3. (A) Velocity distribution of water undergoing laminar flow in a rectangular pipe 3 mm high and 30 mm wide spatially resolved along z. The velocity distribution of each slice was measured using the sequence of Fig. 1 using $\delta = 1$ ms, $\Delta = 50$ ms, field of flow = 40 mm/s, 20 gradient steps, and eight scans per gradient value. To improve the signal-to-noise ratio 2000 echoes were acquired with $t_E = 0.11$ ms. The total experimental time to resolve the velocity distribution was about 30 min. (B) Propagators measured at the center (■), between the center and the wall (●), and next to the wall (▲). It can clearly be observed how the average velocity goes to zero when approaching the wall, while the width of the velocity distribution increases according to the increase in the velocity shear.

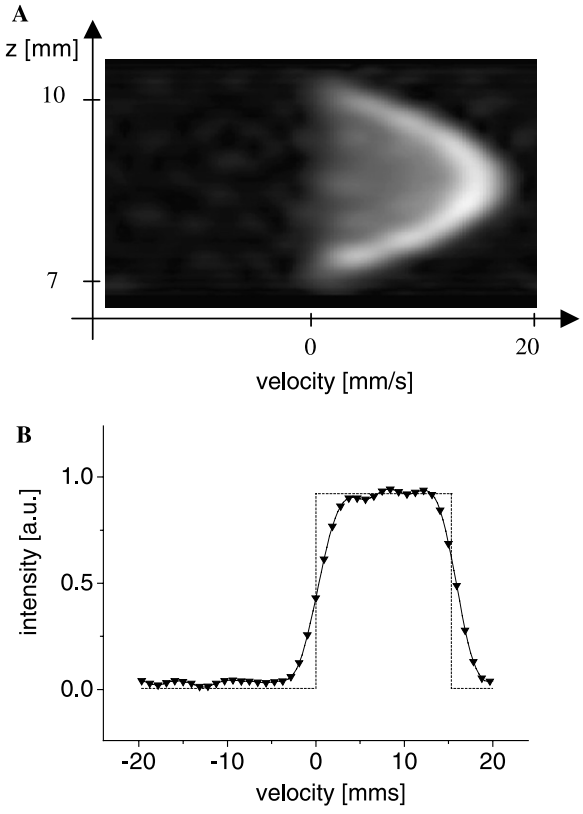

Fig. 4. (A) Velocity distribution of water flowing in a circular pipe, spatially resolved along z. The experimental parameters were the same as the ones used in the experiment of Fig. 3. The flow rate was set to 190 ml/h defining a maximum velocity of 15 mm/s. The maximum velocity as a function of z clearly shows the expected parabolic behavior. (B) Velocity distribution of the complete circular pipe showing the typical hat function correspondent to this geometry. The total velocity distribution was obtained integrating along z the experiment in (A).

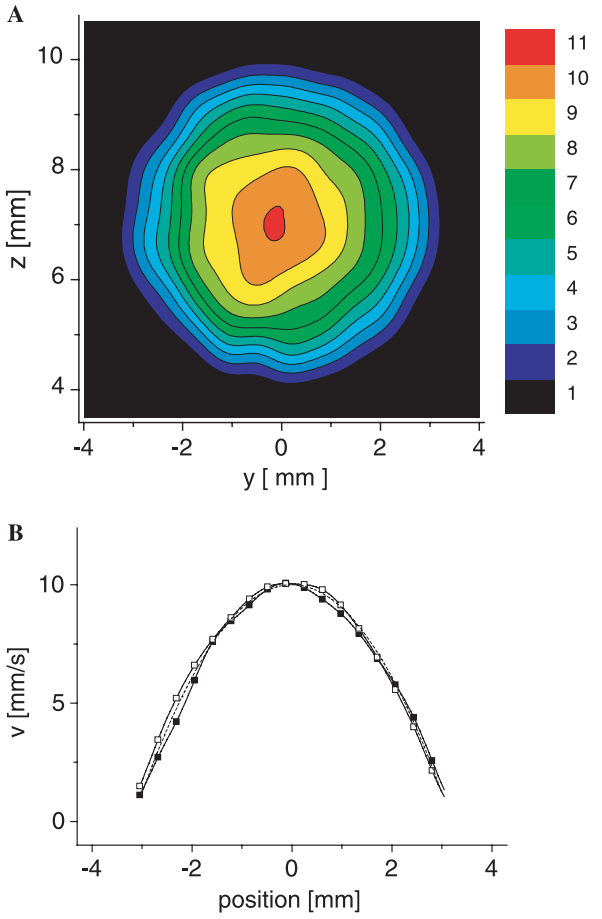

Fig. 5. (A) 2D Velocity map of water flowing in a circular pipe, 6 mm in diameter. It was obtained with the pulse sequence of Fig. 1, using the single gradient step method to encode velocity. The total experimental time to obtain the velocity distribution with the tube placed between 4 and 10 mm from the sensor surface was 50 min. (B) $v(y,0)$ (■), and $v(0,z)$ (□), plotted together with the expected quadratic function (dashed line).

both y and z as $v(y,z) = v_{\max} \times (1-(y^2+z^2)/R^2)$. This defines a velocity distribution in each slice with velocity ranging from zero to a maximum value that depends on the z position. The parabolic behavior of the maximum velocity is clearly resolved in Fig. 4A, which also reveals that the velocity probability is non-zero from zero up to the maximum velocity in the slice. The complete propagator of the tube can be reconstructed by integrating the distributions along the depth. Fig. 4B shows the characteristic hat function expected for this distribution.

3.2. Two-dimensional velocity maps

To spatially resolve the velocity along y a gradient pulse g_y is included as shown in Fig. 1. By combining this sequence with slice selection, the velocity in the y–z plane can be imaged. The method was implemented to map the velocity distribution of a laminar water flow in a circular pipe with 6 mm inner diameter. The flow rate was set to 500 ml/h to define a maximum velocity of about 10 mm/s. The pipe was scanned along z changing the position of the sensitive slice in steps of 0.5 mm. A 1D profile along y of each slice was obtained by increasing the amplitude of the pulsed gradient in 16 steps. Setting a field-of-view of 8 mm, the same spatial resolution along both spatial directions was defined. Fig. 5A shows the 2D velocity map computed from the pixel phase shift measured with the single-step PFG-STE method. The plot clearly shows the annular pattern corresponding to the axially symmetric parabolic velocity distribution developed in this geometry. The agreement of the results with the theoretical profile can be judged in plot 5B, where $v(y,0)$ and $v(0,z)$ are displayed together with the expected quadratic function.

4. Conclusions

A PFG-STE sequence suitable to encode displacement in the presence of strong B_0 and B_1 field gradients

has been combined with imaging techniques to spatially resolve velocity distributions ex situ. It has been successfully implemented on a single-sided NMR sensor with optimized geometry. By taking advantage of the depth selection that can be achieved by retuning the probe frequency, the velocity distribution has been resolved along the depth direction in different pipes. Furthermore, it was demonstrated, that 2D velocity maps can be obtained by combining slice selection with phase encoding imaging. The complete information about fluid dynamics provided non-invasively by ex situ NMR identifies the technique as a powerful tool to monitor on-line flow properties of complex fluids in different processes like extrusion, compression, pumping, mixing, and separation in a variety of geometries. The method is being tested in our laboratory in two important applications. The first is the study of melting processes and the polymer melt flow in a single-screw extruder, and the second is to measure the blood velocity in vivo for evaluation of the blood pressure.

Acknowledgments

Support of this project by the DFG Forschergruppe FOR333 "Surface NMR of Elastomers and Biological Tissue," and the German Federal Ministry of Education and Research (BMBF) within the framework of German–Israeli Project Cooperation (DIP) is gratefully acknowledged.

References

[1] P.T. Callaghan, Principles of Nuclear Magnetic Resonance Microscopy, Clarendon Press, Oxford, 1991.
[2] Y. Xia, P.T. Callaghan, K.R. Jeffrey, Imaging velocity profiles: flow through an abrupt contraction and expansion, A.I.Ch.E. J. 38 (1992) 1408–1420.
[3] B. Blümich, NMR Imaging of Materials, Clarendon Press, Oxford, 2000.
[4] J.D. Seymour, A. Caprihan, S.A. Altobelli, E. Fukushima, Pulsed gradient spin echo nuclear magnetic resonance imaging of diffusion in granular flow, Phys. Rev. Lett. 84 (2) (2000) 266–269.
[5] S. Han, S. Stapf, B. Blümich, NMR imaging of falling water drops, Phys. Rev. Lett. 87 (14) (2001) 144501.
[6] M.D. Mantle, A.J. Sederman, Dynamic MRI in chemical process and reaction engineering, Prog. Nucl. Magn. Reson. Spectrosc. 43 (2003) 3–60.
[7] Y.L. Yeow, J.W. Taylor, Obtaining the shear rate profile of steady laminar tube flow of Newtonian and non-Newtonian fluids from nuclear magnetic resonance imaging and laser Doppler velocimetry data, J. Rheol. 46 (2002) 351–365.
[8] D.F. Arola, R.L. Powell, G.A. Barrall, M.J. McCarthy, Pointwise observations for rheological characterization using nuclear magnetic resonance imaging, J. Rheol. 43 (1999) 9–30.
[9] G. Eidmann, R. Salvelsberg, P. Blümler, B. Blümich, The NMR-MOUSE, a mobile universal surface explorer, J. Magn. Reson. A122 (1996) 104–109.
[10] P.J. Prado, Single sided imaging sensor, Magn. Reson. Imaging 21 (2003) 397–400.
[11] R.L. Kleinberg, Well logging, in: D.M. Grant, R.K. Harris (Eds.), Encyclopedia of NMR, Wiley, New York, 1996, pp. 4960–4969.
[12] US Patent 5,959,454. Bruker Analytic. Magnet arrangement for an NMR tomography system, in particular for skin and surface examinations.
[13] J. Perlo, F. Casanova, B. Blümich, 3D imaging with a single-sided sensor: an open tomograph, J. Magn. Reson. 166 (2004) 228–235.
[14] M.D. Hürlimann, M. Flaum, L. Venkataramanan, C. Flaum, R. Freedman, G.J. Hirasaki, Diffusion-relaxation distribution functions of sedimentary rocks in different saturation states, Magn. Reson. Imaging 21 (2003) 305–510.
[15] F. Casanova, J. Perlo, B. Blümich, Velocity distributions remotely measured with a single-sided sensor, J. Magn. Reson. 171 (2004) 124–130.
[16] J.E. Tanner, Use of the stimulated echo in NMR diffusion studies, J. Chem. Phys. 52 (1970) 2523–2526.
[17] R.M. Cotts, M.J.R. Hoch, T. Sun, J.T. Markert, Pulsed field gradient stimulated echo methods for improved NMR diffusion measurements in heterogeneous systems, J. Magn. Reson. 83 (1989) 252–266.
[18] Y. Xia, P.T. Callaghan, One-Shot velocity microscopy: NMR imaging of motion using a single phase-encoding step, Magn. Reson. Med. 23 (1992) 138–153.